

## Article

# Dynamic Modeling and Vibration Characteristics Analysis of Deep-Groove Ball Bearing, Considering Sliding Effect

Fanjie Li, Xiaopeng Li \*  and Dongyang Shang

School of Mechanical Engineering and Automation, Northeastern University, Shenyang 110819, China; fanjieli2021@163.com (F.L.); dongyangshangneu@163.com (D.S.)

\* Correspondence: xpli@me.neu.edu.cn

**Abstract:** To study the vibration characteristics of deep-groove ball bearing, considering the influence of sliding, the dynamic model of the DGB 6205 system is established in this paper. The DGB 6205 system model includes the movement of the bearing inner ring in the  $X$  and  $Y$  directions, the rotation of the cage, the rotation movement of each ball, the revolution movement of each ball and the movement along the radial direction of each ball. Based on the system model, the differential equations of motion of the system are established, and the correctness of the model is verified by experiment. The slip characteristics of the DGB 6205 system are studied by numerical simulation. At the same time, the influence of time-varying load on the vibration characteristics of the system is studied. Then, the sensitivity of system parameters is analyzed. The results show that the sliding speed between the ball and the inner raceway is greater than that between the ball and the outer raceway. The radial vibration response of DGB 6205 system under time-varying load is less than that under constant load. The increase of radial clearance will increase the vibration response of DGB 6205 system.



**Citation:** Li, F.; Li, X.; Shang, D. Dynamic Modeling and Vibration Characteristics Analysis of Deep-Groove Ball Bearing, Considering Sliding Effect. *Mathematics* **2021**, *9*, 2408. <https://doi.org/10.3390/math9192408>

Academic Editor: Vasyil Martsenyuk

Received: 28 August 2021  
Accepted: 22 September 2021  
Published: 28 September 2021

**Publisher's Note:** MDPI stays neutral with regard to jurisdictional claims in published maps and institutional affiliations.



**Copyright:** © 2021 by the authors. Licensee MDPI, Basel, Switzerland. This article is an open access article distributed under the terms and conditions of the Creative Commons Attribution (CC BY) license (<https://creativecommons.org/licenses/by/4.0/>).

**Keywords:** dynamics; deep-groove ball bearing; sliding effect; parameter sensitivity; time-varying load; vibration characteristics

## 1. Introduction

As the main supporting component of aeroengine and motor, the bearing plays an increasingly important role. The sliding effect is an objective phenomenon in the working process of bearing. It is caused by insufficient drag force in the bearing caused by environment and physical contact force. The sliding effect will increase the temperature at the contact between the rolling element and the raceway, aggravate the bearing wear, and then shorten the bearing fatigue life. Therefore, it is important to establish the dynamic model and analyze the vibration characteristics of the bearing, while considering the sliding effect.

Harris [1,2] proposed a bearing slip prediction method for the first time, in view of the sliding effect during bearing operation. Gupta [3,4] considered the interaction between the rolling element and the cage in the theoretical model and analyzed the motion characteristics of the bearing. Considering that the common contact between the ball and the inner and outer raceways of the bearing has significant curvature, the differential sliding quasi-static model was established [5,6]. Considering the influence of centrifugal force, the sliding characteristics of bearing under radial load and axial load were studied [7]. Tu et al. [8] proposed a model to study the sliding behavior of bearing during accelerated operation. However, this model does not consider the influence of bearing radial clearance on the sliding behavior. Shi et al. [9] proposed an improved two-dimensional bearing dynamic model to calculate the vibration response of cylindrical roller bearing. However, this model does not consider the influence of bearing sliding effect on vibration response. Han and Chu [10] established the mechanical model of angular contact ball bearing under combined load. Lin et al. [11] proposed an intelligent bearing diagnosis system and

analyzed the fault response of the bearing system. The literature [12–14] used the deep learning algorithm to quickly and accurately predict the remaining service life of bearings. Zhu et al. [15] proposed a transfer learning method based on multilayer perceptron to predict the remaining life of bearing under different working conditions. Li et al. [16] established the contact mechanics model of flexible bearing and analyzed the motion characteristics of flexible bearing. Liu et al. [17,18] proposed a bearing dynamic model, considering the influence of defects, and applied the model to study the influence of defect morphology on bearing contact characteristics. The influence of various types of bearing local surface defects on the vibration response of bearing system was studied [19–21]. Cao et al. [22] established the dynamic model of cylindrical roller bearing based on the model proposed by Gupta and studied the vibration mechanism of bearing with local defects. Ghafari et al. [23] studied the influence of local fault on chaotic vibration of bearing system. Qin et al. [24] proposed a new fault bearing model and analyzed the acceleration response, considering the influence of local surface defects. However, most of the existing studies are based on bearing system quasi-static analysis, bearing fault diagnosis and life prediction based on deep learning, and dynamic analysis considering bearing macro defect.

In this paper, the dynamic model of DGB 6205 system comprehensively considers the effects of bearing sliding friction, radial clearance, speed, load change, and so on. The purpose of this paper is to study the vibration characteristics of DGB 6205 system by considering the sliding effect under different operating conditions.

The structure of the paper is as follows. In Section 2, the dynamic model of the DGB 6205 system, considering sliding effect, is established. In Section 3, the correctness of the model is verified by comparing the experimental results with the theoretical simulation results. In Section 4, the slip characteristics of the DGB 6205 system, the influence of time-varying load on the characteristics of the DGB 6205 system, and the parameter sensitivity of the dynamic response of the DGB 6205 system are analyzed, respectively. Finally, the conclusions of this paper are given in Section 5.

## 2. Dynamic Modeling of the DGB 6205 System

To analyze the dynamic characteristics of the DGB 6205 system in slip state, the dynamic modeling of the DGB 6205 system was carried out. The physical drawing of the DGB 6205 is shown in Figure 1.

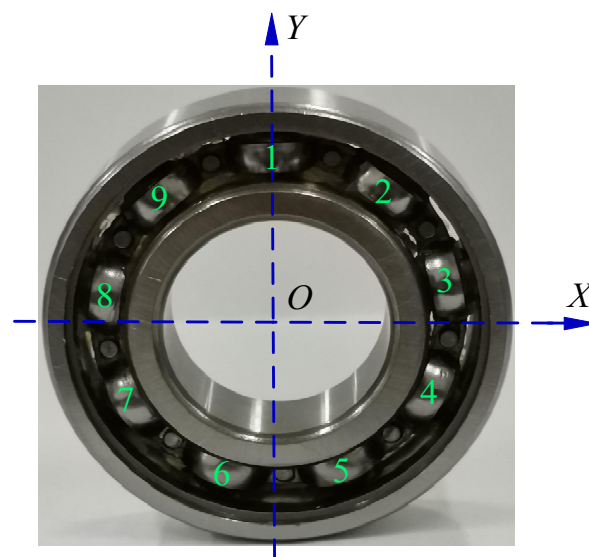


Figure 1. Physical drawing of the DGB 6205.

In Figure 1, the DGB 6205 has 9 rolling elements, and the numbers 1–9 represent the roller number respectively. The center of the bearing inner race is taken as the coordinate

origin  $O$ ; the horizontal direction passing through the coordinate origin is the  $X$ -axis, and the vertical direction is the  $Y$ -axis.

2.1. Equivalent Model of the DGB 6205 System

By using an equivalent model of the DGB 6205 system’s physical model, the kinematic relationship of the model is obtained. This paper assumes that the bearing is installed on a rigid shaft. The kinematic relationship model of the DGB 6205 system is shown in Figure 2.

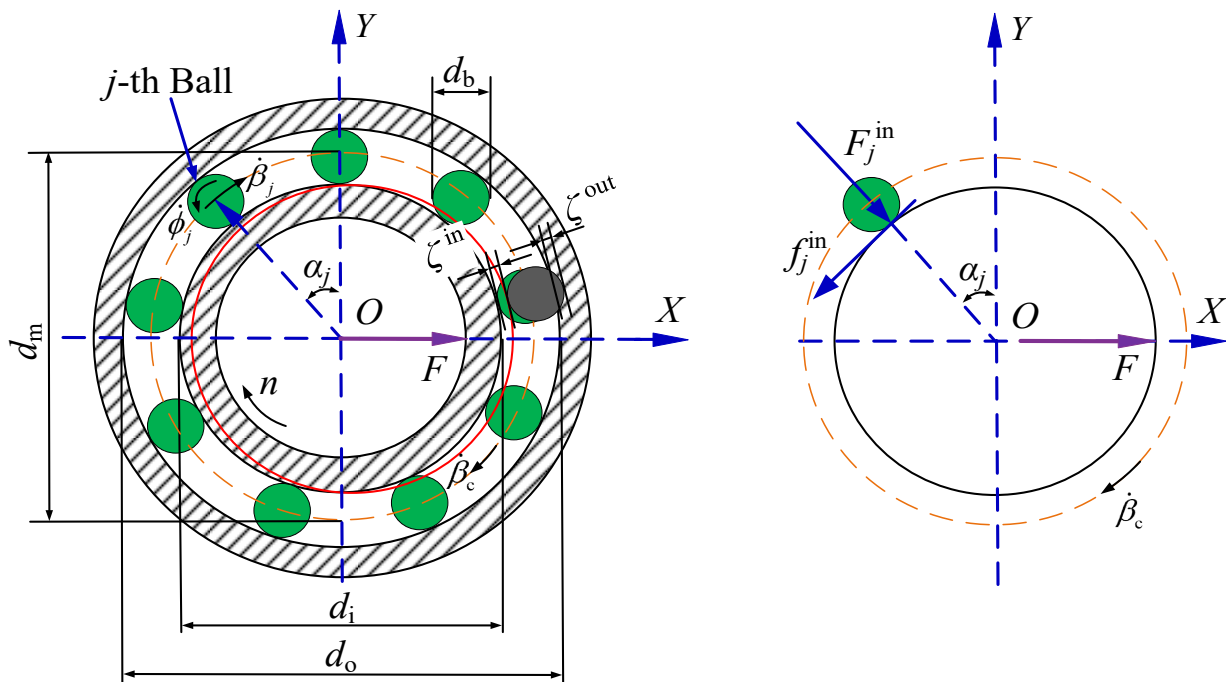


Figure 2. Kinematic relationship model of the DGB 6205 system.

In Figure 2,  $\alpha_j$  is the position angle of the  $j$ -th ball in DGB 6205,  $\dot{\phi}_j$  is the rotation speed of the  $j$ -th ball in DGB 6205,  $\dot{\beta}_j$  is the revolution speed of the  $j$ -th ball in DGB 6205, and  $\dot{\beta}_c$  is the rotation speed of the cage in DGB 6205.  $F$  is the radial load acting on the inner race, and  $n$  is the rotational speed of the inner race.  $\zeta^{in}$  is the contact deformation between ball and inner raceway, and  $\zeta^{out}$  is the contact deformation between ball and outer raceway. Moreover,  $d_i$  is the diameter of inner raceway,  $d_o$  is the diameter of outer raceway,  $d_m$  is the pitch diameter, and  $d_b$  is the ball diameter.  $F_j^{in}$  is the contact force between the  $j$ -th ball and the inner race, and  $f_j^{in}$  is the friction force between the  $j$ -th ball and the inner race. The position angle  $\alpha_j$  of the  $j$ -th ball in the 6205 bearing can be written as follows:

$$\alpha_j = \dot{\beta}_j t + \alpha_0 + \frac{2\pi(j-1)}{Z}, \quad (j = 1, 2, \dots, Z). \tag{1}$$

where  $Z$  is the number of balls in DGB 6205 system,  $\alpha_0$  is the initial angle, and  $\alpha_0$  is set to be zero.

To more clearly represent the contact state between the ball and the inner and outer raceways and the contact state between the ball and the cage during the operation of the bearing, the contact stiffness model of the DGB 6205 is established. The contact stiffness model of the DGB 6205 is shown in Figure 3.

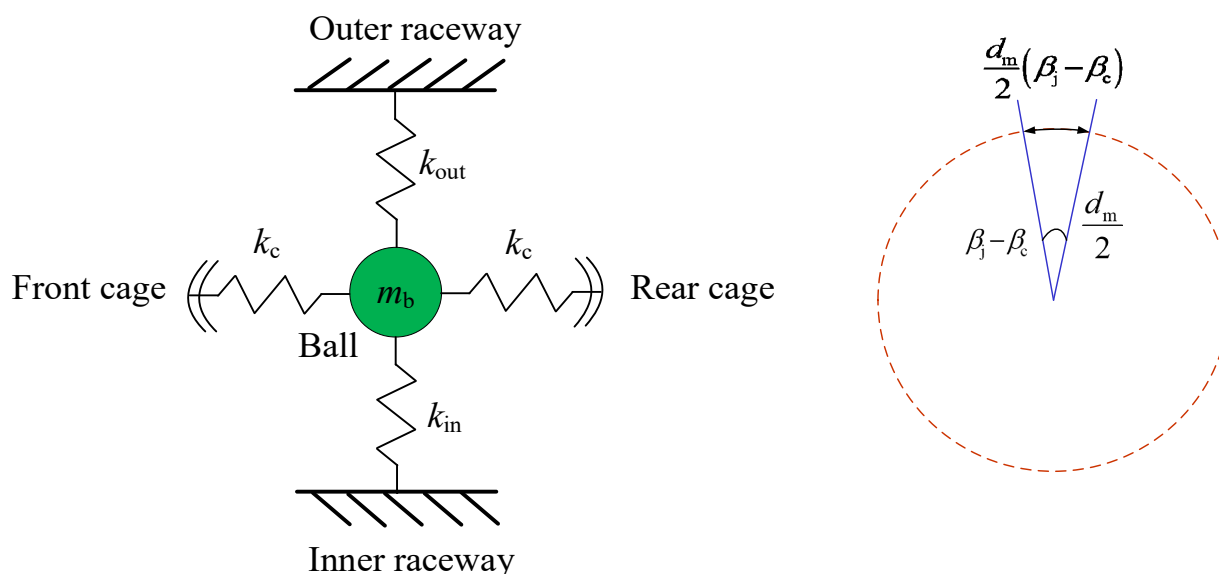


Figure 3. Contact-stiffness model of the DGB 6205.

In Figure 3,  $m_b$  is the mass of the ball in DGB 6205,  $k_{in}$  is the contact stiffness between ball and inner raceway,  $k_{out}$  is the contact stiffness between ball and outer raceway, and  $k_c$  is the contact stiffness between cage and ball. The ball in deep-groove ball bearing is made of bearing steel. The mass of the ball can be obtained by multiplying the volume and density of the ball. The mass  $m_b$  of the ball can be written as follows:

$$m_b = \frac{4}{3}\pi\left(\frac{d_b}{2}\right)^3 \rho \tag{2}$$

where  $d_b$  is the ball diameter in DGB 6205 system, and  $\rho$  is the density of bearing steel.

The parameters of the model come from a DGB 6205 bearing, and the model parameters of the DGB 6205 are shown in Table 1.

Table 1. Model parameters of the DGB 6205.

Item	Notation	Value
Number of balls	$Z$	9
Diameter of outer raceway	$d_o$	45.84 mm
Diameter of inner raceway	$d_i$	33.16 mm
Pitch diameter of bearing	$d_m$	39.50 mm
Ball diameter	$d_b$	6.34 mm
Mass of inner race and shaft	$m_s$	0.825 kg
Density of bearing steel	$\rho$	7810 kg/m <sup>3</sup>
Moment of inertia of cage	$I_c$	$0.86 \times 10^{-6}$ kg·m <sup>2</sup>
Contact stiffness between ball and inner raceway	$k_{in}$	$3.18 \times 10^{10}$ N/m
Contact stiffness between ball and outer raceway	$k_{out}$	$3.36 \times 10^{10}$ N/m
Contact stiffness between cage and ball	$k_c$	$6.06 \times 10^9$ N/m
Gravitational acceleration	$g$	9.8 m/s <sup>2</sup>
Radial clearance	$p$	10 μm
Friction coefficient between cage and ball	$\mu_c$	0.002

In Table 1, the friction coefficient  $\mu_c$  describes kinetic friction. The subscript c in the moment of inertia  $I_c$  of the cage represents the meaning of the cage.

### 2.2. Differential Equations of Motion of the DGB 6205 System

The differential equations of motion of the system are often used to describe the dynamic characteristics of the system. The dynamic response of the system can be obtained

by solving the differential equations of motion of the system by the fourth-order Runge–Kutta method. The fourth-order Runge–Kutta method has high accuracy and can effectively suppress the error. The fourth-order Runge–Kutta method is a high-precision one-step algorithm that is widely used in engineering.

The equation of motion of the system inner race in the  $X$  direction can be written as follows:

$$m_s \ddot{x} = F + \sum_{j=1}^Z (F_j^{\text{in}} \sin \alpha_j - f_j^{\text{in}} \cos \alpha_j) \tag{3}$$

where  $F$  is the radial load acting on the inner race,  $m_s$  is the mass of inner race and shaft,  $\ddot{x}$  is the acceleration of the inner race in the  $X$  direction,  $F_j^{\text{in}}$  is the contact force between the  $j$ -th ball and the inner race, and  $f_j^{\text{in}}$  is the friction force between the  $j$ -th ball and the inner race.

The equation of motion of the DGB 6205 system inner race in the  $Y$  direction can be written as follows:

$$m_s \ddot{y} = - \sum_{j=1}^Z (F_j^{\text{in}} \cos \alpha_j + f_j^{\text{in}} \sin \alpha_j) \tag{4}$$

where  $\ddot{y}$  is the acceleration of the inner race in the  $Y$  direction.

The contact force between the  $j$ -th ball and the inner race can be written as follows [9]:

$$F_j^{\text{in}} = k_{\text{in}} (\zeta_j^{\text{in}} \gamma_j^{\text{in}})^{3/2} \tag{5}$$

where  $k_{\text{in}}$  is the contact stiffness between ball and inner raceway,  $\zeta_j^{\text{in}}$  is the contact deformation between the  $j$ -th ball and inner raceway, and  $\gamma_j^{\text{in}}$  is the deformation function of the  $j$ -th ball in contact with the inner raceway.

The contact deformation between the  $j$ -th ball and inner raceway can be written as follows:

$$\zeta_j^{\text{in}} = x \sin \alpha_j + y \cos \alpha_j - d_j - \frac{p}{2} \tag{6}$$

where  $x$  is the displacement of the inner race in the  $X$  direction,  $y$  is the displacement of the inner race in the  $Y$  direction,  $d_j$  is the  $j$ -th ball radial displacement, and  $p$  is the radial clearance.

The deformation function of the  $j$ -th ball in contact with the inner raceway can be written as follows:

$$\gamma_j^{\text{in}} = \begin{cases} 1 & \zeta_j^{\text{in}} > 0, \\ 0 & \zeta_j^{\text{in}} \leq 0. \end{cases} \tag{7}$$

The contact force between the  $j$ -th ball and outer raceway can be written as follows [9]:

$$F_j^{\text{out}} = k_{\text{out}} (\zeta_j^{\text{out}} \gamma_j^{\text{out}})^{3/2} \tag{8}$$

where  $k_{\text{out}}$  is the contact stiffness between ball and outer raceway,  $\zeta_j^{\text{out}}$  is the contact deformation between the  $j$ -th ball and outer raceway, and  $\gamma_j^{\text{out}}$  is the deformation function of the  $j$ -th ball in contact with the outer raceway.

The contact deformation between the  $j$ -th ball and outer raceway can be written as follows:

$$\zeta_j^{\text{out}} = d_j - \frac{p}{2} \tag{9}$$

The deformation function of the  $j$ -th ball in contact with the outer raceway can be written as follows:

$$\gamma_j^{\text{out}} = \begin{cases} 1 & \zeta_j^{\text{out}} > 0, \\ 0 & \zeta_j^{\text{out}} \leq 0. \end{cases} \tag{10}$$

The friction force between the  $j$ -th ball and the inner race can be written as follows:

$$f_j^{\text{in}} = -\text{sign}(\Delta v_j^{\text{in}}) \mu_j^{\text{in}} F_j^{\text{in}} \tag{11}$$

where  $\Delta v_j^{\text{in}}$  is the sliding speed between the  $j$ -th ball and the inner race, and  $\mu_j^{\text{in}}$  is the kinetic friction coefficient between the  $j$ -th ball and the inner race.

The sliding speed between the  $j$ -th ball and the inner race can be written as follows:

$$\Delta v_j^{\text{in}} = \left( \frac{2\pi n}{60} - \dot{\beta}_c \right) \frac{d_i}{2} - \dot{\phi}_j \frac{d_b}{2} \tag{12}$$

The friction coefficient between the  $j$ -th ball and the inner race can be written as follows [25]:

$$\mu_j^{\text{in}} = \begin{cases} 0.04 |\Delta v_j^{\text{in}}| & |\Delta v_j^{\text{in}}| < 0.05, \\ 0.002 & |\Delta v_j^{\text{in}}| \geq 0.05. \end{cases} \tag{13}$$

The friction force between the  $j$ -th ball and the outer race can be written as follows:

$$f_j^{\text{out}} = -\text{sign}(\Delta v_j^{\text{out}}) \mu_j^{\text{out}} F_j^{\text{out}} \tag{14}$$

where  $\Delta v_j^{\text{out}}$  is the sliding speed between the  $j$ -th ball and the outer race, and  $\mu_j^{\text{out}}$  is the friction coefficient between the  $j$ -th ball and the outer race.

The sliding speed between the  $j$ -th ball and the outer race can be written as follows:

$$\Delta v_j^{\text{out}} = \dot{\beta}_c \frac{d_o}{2} - \dot{\phi}_j \frac{d_b}{2} \tag{15}$$

The friction coefficient between the  $j$ -th ball and the outer race can be written as follows:

$$\mu_j^{\text{out}} = \begin{cases} 0.04 |\Delta v_j^{\text{out}}| & |\Delta v_j^{\text{out}}| < 0.05, \\ 0.002 & |\Delta v_j^{\text{out}}| \geq 0.05. \end{cases} \tag{16}$$

The radial equation of motion of the  $j$ -th ball in DGB 6205 system can be written as follows:

$$m_b \ddot{d}_j = m_b g \cos \alpha_j + F_j^{\text{in}} - F_j^{\text{out}} - F_j^{\text{cf}} + F_j^{\text{cr}} + m_b \frac{d_m}{2} \dot{\beta}_j^2 \tag{17}$$

where  $\ddot{d}_j$  is the radial acceleration of the  $j$ -th ball,  $g$  is the gravitational acceleration,  $F_j^{\text{cf}}$  is the contact force between the  $j$ -th ball and the front cage, and  $F_j^{\text{cr}}$  is the contact force between the  $j$ -th ball and the rear cage.

The contact force between the  $j$ -th ball and the front cage can be written as follows:

$$F_j^{\text{cf}} = \begin{cases} k_c \frac{d_m}{2} (\beta_j - \beta_c) & (\beta_j - \beta_c) > 0, \\ 0 & (\beta_j - \beta_c) \leq 0. \end{cases} \tag{18}$$

where  $k_c$  is the contact stiffness between the cage and ball,  $\beta_j$  is the revolution angle of the  $j$ -th ball in DGB 6205, and  $\beta_c$  is the rotation angle of the cage in DGB 6205.

The contact force between the  $j$ -th ball and the rear cage can be written as follows:

$$F_j^{\text{cr}} = \begin{cases} k_c \frac{d_m}{2} (\beta_c - \beta_j) & (\beta_c - \beta_j) > 0, \\ 0 & (\beta_c - \beta_j) \leq 0. \end{cases} \tag{19}$$

The equation of motion of the rotation direction of the  $j$ -th ball in the DGB 6205 system can be written as follows:

$$m_b \left(\frac{d_b}{2}\right)^2 \ddot{\phi}_j = (f_j^{\text{in}} + f_j^{\text{out}}) \frac{d_b}{2} - (f_j^{\text{cf}} + f_j^{\text{cr}}) \frac{d_b}{2} \tag{20}$$

where  $\ddot{\phi}_j$  is the rotation acceleration of the  $j$ -th ball in DGB 6205,  $f_j^{\text{cf}}$  is the friction force between the  $j$ -th ball and the front cage, and  $f_j^{\text{cr}}$  is the friction force between the  $j$ -th ball and the rear cage.

The friction force between the  $j$ -th ball and the front cage can be written as follows:

$$f_j^{\text{cf}} = \mu_c F_j^{\text{cf}} \tag{21}$$

where  $\mu_c$  is the friction coefficient between cage and ball.

The friction force between the  $j$ -th ball and the rear cage can be written as follows:

$$f_j^{\text{cr}} = \mu_c F_j^{\text{cr}} \tag{22}$$

The equation of motion of the revolution direction of the  $j$ -th ball in DGB 6205 system can be written as follows:

$$m_b \frac{d_m}{2} \ddot{\beta}_j = -m_b g \sin \alpha_j + f_j^{\text{in}} - f_j^{\text{out}} - f_j^{\text{cf}} + f_j^{\text{cr}} \tag{23}$$

where  $\ddot{\beta}_j$  is the revolution acceleration of the  $j$ -th ball in the DGB 6205.

The equation of the motion of the cage rotation direction in the DGB 6205 system can be written as follows:

$$sI_c \ddot{\beta}_c = \frac{d_m}{2} \sum_{j=1}^Z (F_j^{\text{cf}} - F_j^{\text{cr}}) \tag{24}$$

where  $I_c$  is the moment of inertia of cage, and  $\ddot{\beta}_c$  is the rotation acceleration of the cage in DGB 6205.

Equations (3), (4), (17), (20), (23) and (24) are combined into Equation (25), and the differential equations of motion of the DGB 6205 system can be written as follows:

$$\begin{cases} \ddot{x} = \frac{1}{m_s} \left[ F + \sum_{j=1}^Z (F_j^{\text{in}} \sin \alpha_j - f_j^{\text{in}} \cos \alpha_j) \right] \\ \ddot{y} = \frac{1}{m_s} \left[ -\sum_{j=1}^Z (F_j^{\text{in}} \cos \alpha_j + f_j^{\text{in}} \sin \alpha_j) \right] \\ \ddot{d}_j = \frac{1}{m_b} \left( m_b g \cos \alpha_j + F_j^{\text{in}} - F_j^{\text{out}} - F_j^{\text{cf}} + F_j^{\text{cr}} + m_b \frac{d_m}{2} \dot{\beta}_j^2 \right) \\ \ddot{\phi}_j = \frac{4}{m_b d_b^2} \left[ (f_j^{\text{in}} + f_j^{\text{out}}) \frac{d_b}{2} - (f_j^{\text{cf}} + f_j^{\text{cr}}) \frac{d_b}{2} \right] \\ \ddot{\beta}_j = \frac{2}{m_b d_m} \left( -m_b g \sin \alpha_j + f_j^{\text{in}} - f_j^{\text{out}} - f_j^{\text{cf}} + f_j^{\text{cr}} \right) \\ \ddot{\beta}_c = \frac{1}{I_c} \left[ \frac{d_m}{2} \sum_{j=1}^Z (F_j^{\text{cf}} - F_j^{\text{cr}}) \right] \end{cases} \tag{25}$$

### 3. Experimental Verification

To verify the dynamic model established in this paper, the dynamic responses of DGB 6205 system under different radial loads are measured by an ABLT-1A bearing experimental machine. The experimental results of DGB 6205 system are compared with the theoretical results.

The ABLT-1A bearing experimental machine is shown in Figure 4.

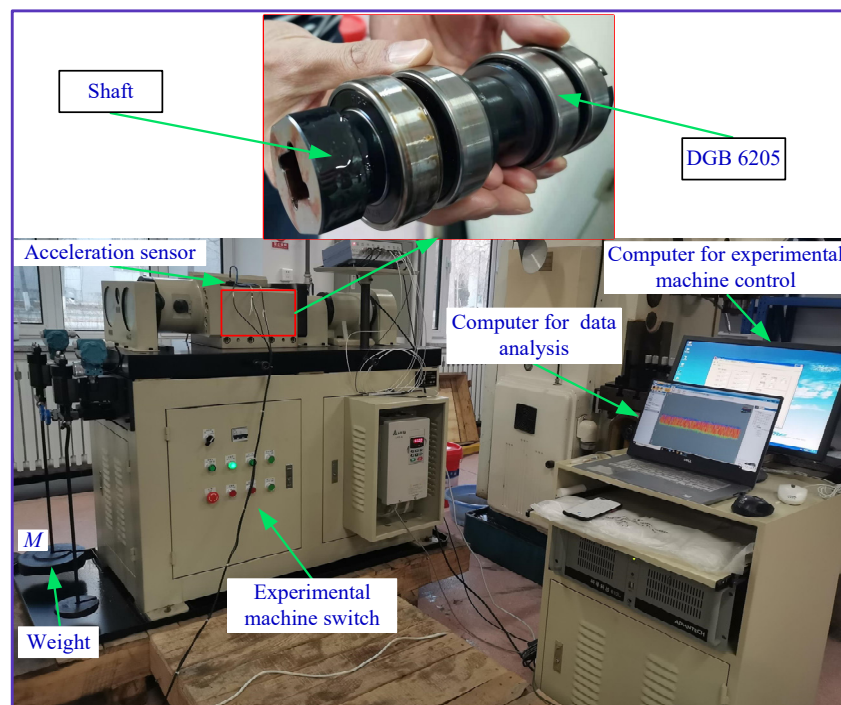


Figure 4. ABLT-1A bearing experimental machine.

Figure 4 illustrates that the ABLT-1A bearing experimental machine is mainly composed of a test head, test head seat, transmission system, loading system, lubrication system, electrical control system, computer, and so on. Four bearings of the same size are installed on the shaft in parallel, and the shaft is installed in the test head. After the power is turned on, we first start the experimental machine through the experimental machine switch, then set the motor speed through the computer for experimental machine control, and finally collect the radial vibration signal of DGB 6205 system through the computer for data analysis.

In the experiment, the motor speed is set to 3000 rpm; that is, the rotational speed of the 6205 bearing inner race is 3000 rpm. The mass  $M$  of the weight is 5 and 10 kg, respectively, and the vibration response of DGB 6205 under different radial loads is obtained. The radial vibration acceleration response of DGB 6205 under different radial loads is shown in Figure 5.

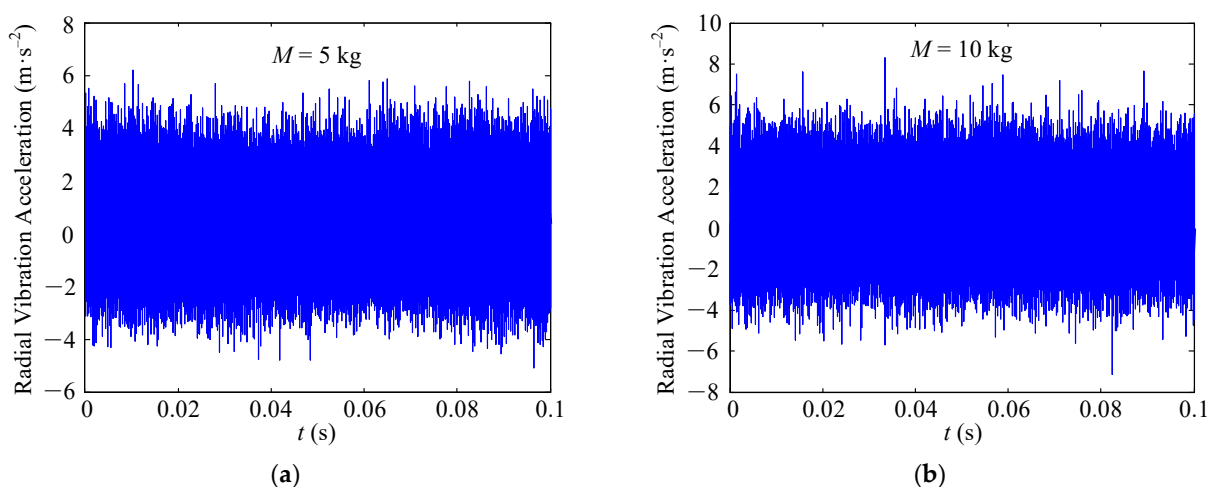
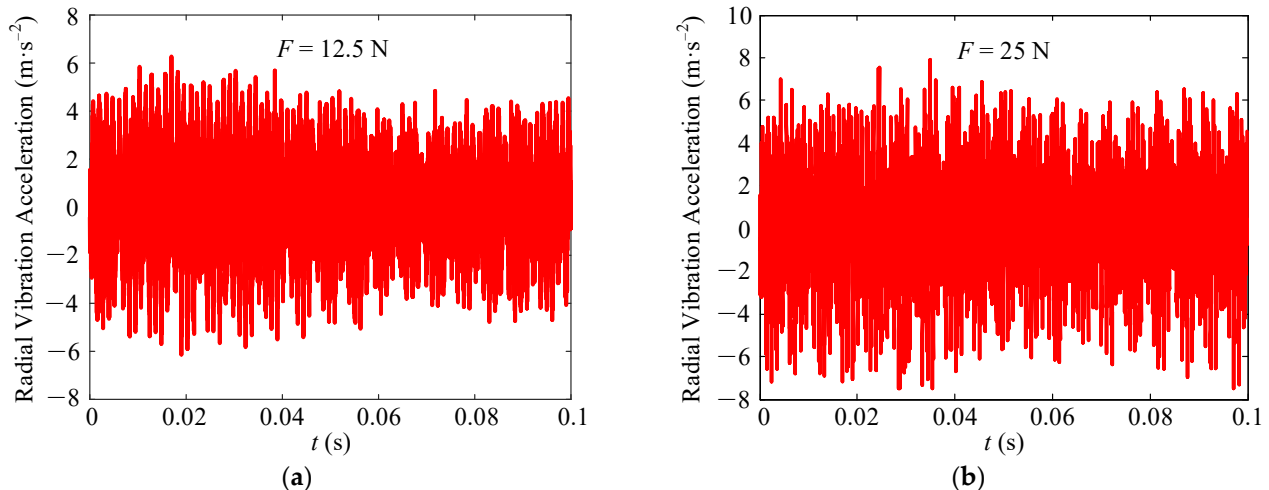


Figure 5. Radial vibration acceleration response of DGB 6205 under different radial loads: (a) radial vibration acceleration under 5 kg weight and (b) radial vibration acceleration under 10 kg weight.

In Figure 5, the root mean square value of the radial vibration acceleration of the DGB 6205 system under a weight of 5 kg is  $1.36 \text{ m}\cdot\text{s}^{-2}$ , and the root mean square value of radial vibration acceleration of the DGB 6205 system under a weight of 10 kg is  $1.58 \text{ m}\cdot\text{s}^{-2}$ . The experimental results show that the vibration response of the DGB 6205 system increases with the increase of radial load.

Under the same working conditions, the radial vibration acceleration response obtained by the theoretical simulation is shown in Figure 6.



**Figure 6.** Radial vibration acceleration response obtained by theoretical simulation: (a) radial vibration acceleration under 12.5 N load and (b) radial vibration acceleration under 25 N load.

In Figure 6, the root-mean-square value of radial vibration acceleration of the DGB 6205 system under 12.5 N load is  $2.12 \text{ m}\cdot\text{s}^{-2}$ , and the root-mean-square value of the radial vibration acceleration of the DGB 6205 system under 25 N load is  $2.41 \text{ m}\cdot\text{s}^{-2}$ . The theoretical simulation results show that the vibration response of the DGB 6205 system increases with the increase of radial load. Therefore, the theoretical simulation results are consistent with the experimental results, thus verifying the correctness of the dynamic model established in this paper.

#### 4. Results and Discussion

Based on the dynamic model of the DGB 6205 system established in this paper, the slip characteristics of the system, the influence law of time-varying load on the dynamic characteristics of the system, and the sensitivity of parameters are studied through numerical simulation. Firstly, the sliding speed between the ball and the inner raceway and outer raceway and the influence of different speeds are analyzed. Then, the vibration response of DGB 6205 system is studied in the time domain and frequency domain, respectively. Finally, the variation of radial displacement and radial vibration acceleration with parameters is discussed. The flowchart of numerical simulation is shown in Figure 7.

##### 4.1. Analysis of Slip Characteristics of DGB 6205 System

During the operation of the bearing, the sliding fault often occurs. The bearing is the main supporting component of the aeroengine and high-speed motor. Bearing slip fault will seriously affect the performance, working reliability, and service life of equipment. Therefore, the slip characteristics of the DGB 6205 system are analyzed in this paper. The sliding speed between the ball and the inner raceway and outer raceway is shown in Figure 8.

In Figure 8, the sliding speed between the ball and the inner raceway is greater than that between the ball and the outer raceway, because the inner ring rotates and the outer ring remains stationary during the operation of DGB 6205 system. At the same time, as the position angle  $\alpha_j$  of the ball in DGB 6205 system increases from 0 to  $2\pi$  rad, the sliding

speed between the ball and the inner raceway and outer raceway decreases first and then increases. The position where the minimum sliding speed occurs is the load action position, and the difference between the position where the maximum sliding speed occurs and the load action position is  $\pi$  rad, indicating that the sliding speed of the ball and the inner and outer raceways gradually decreases with the increase of load  $F$ .

The sliding speed between the ball and the raceway is affected not only by the load  $F$ , but also by the speed  $n$ . Because the sliding degree between the ball and the inner raceway is high, the influence of different rotating speeds on the sliding speed between the ball and the inner raceway in DGB 6205 system is analyzed.

The sliding speed between the ball and the inner raceway at different speeds is shown in Figure 9.

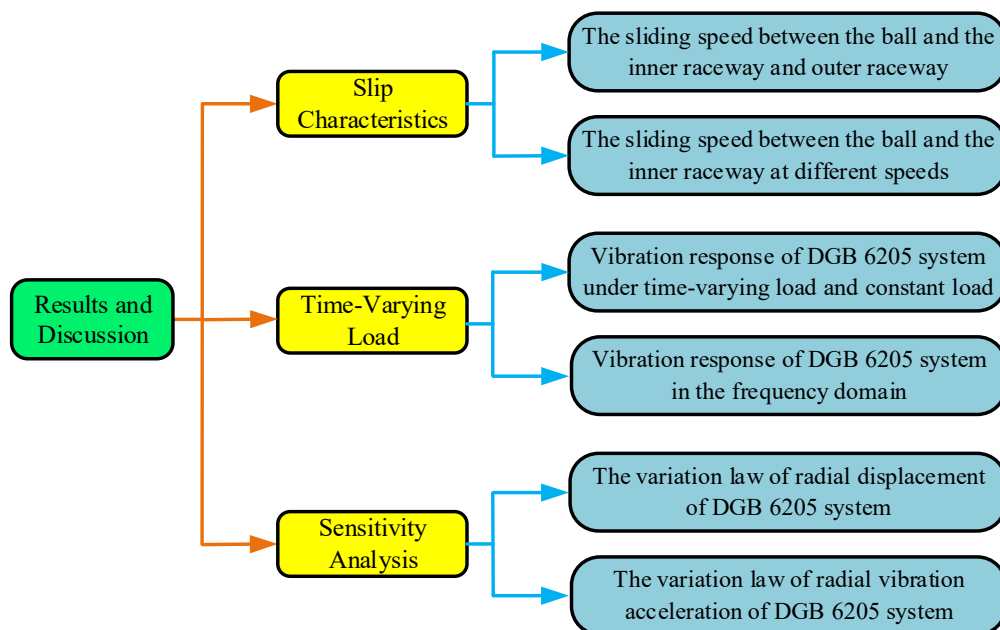


Figure 7. Flowchart of numerical simulation.

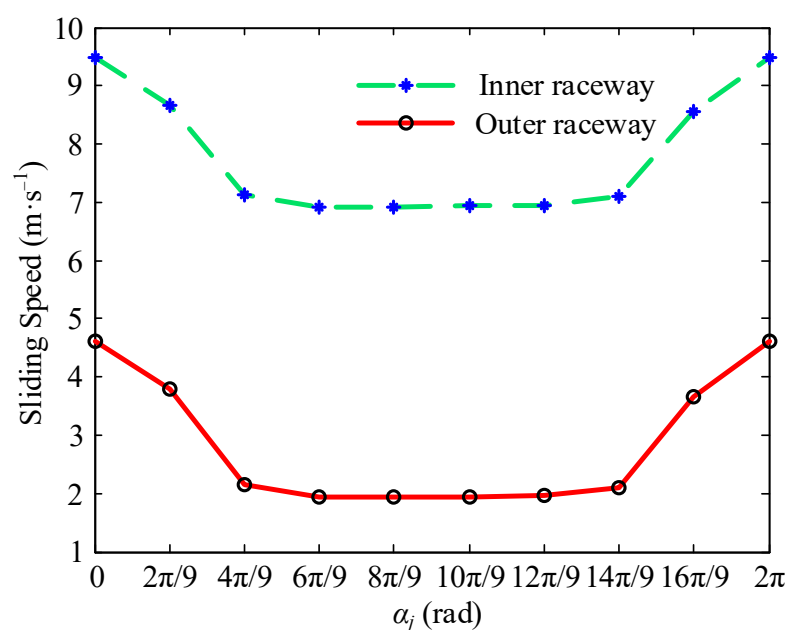


Figure 8. Sliding speed between the ball and the inner raceway and outer raceway.

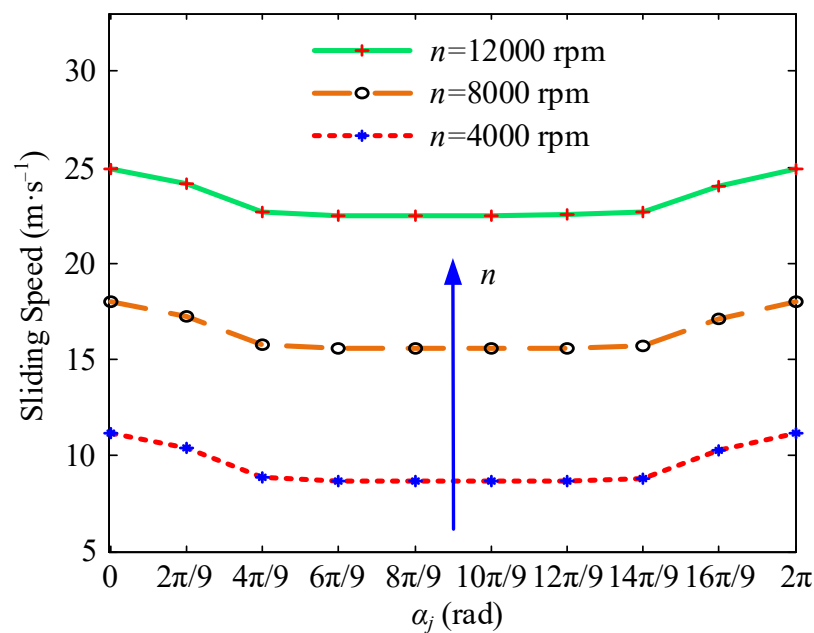


Figure 9. Sliding speed between the ball and the inner raceway at different speeds.

In Figure 9, as the speed  $n$  increases from 4000 to 12,000 rpm, the sliding speed between the ball and the inner raceway in the DGB 6205 system increases, indicating that the increase of speed  $n$  will lead to the increase of sliding speed, and the DGB 6205 system is more prone to slip at high speed.

#### 4.2. Influence of Time-Varying Load on the Characteristics of DGB 6205 System

During the operation of bearing rotor system, the load is often not constant. The time-varying load will have an important impact on the dynamic performance of the bearing rotor system. It is necessary to analyze the influence law of the time-varying load on the bearing rotor system.

The time-varying load acting on DGB 6205 system can be written as follows:

$$F_t = F \sin\left(\frac{2\pi n}{60}t\right) \tag{26}$$

The differential equations of motion of the DGB 6205 system are solved, and the vibration responses of the DGB 6205 system under time-varying load and constant load are obtained, respectively. The vibration response of the DGB 6205 system under time-varying load and constant load is shown in Figure 10 for when the radial load  $F$  is 20 N and the rotational speed of the inner race  $n$  is 6000 rpm.

In Figure 10, compared with the constant load condition, the radial vibration response of DGB 6205 system under time-varying load is smaller. In the  $X$  direction, the root mean square value of radial vibration acceleration decreases from 20.17 to 11.81  $\text{m}\cdot\text{s}^{-2}$ . In the  $Y$  direction, the root mean square value of the radial vibration acceleration decreases from 2.20 to 1.81  $\text{m}\cdot\text{s}^{-2}$ . The vibration response of the DGB 6205 system in the  $X$  direction is greater than that in the  $Y$  direction, because the radial load acts in the  $X$  direction.

The vibration response of the DGB 6205 system under the time-varying load and constant load shown in Figure 10 is subjected to FFT. The vibration response of the DGB 6205 system under time-varying load and constant load in the frequency domain after FFT is shown in Figure 11.

In Figure 11, it is obvious that the amplitude of vibration response of the DGB 6205 system under time-varying load is less than that under constant load. In the  $X$  direction, the amplitude decreases from 22.46 to 9.78  $\text{m}\cdot\text{s}^{-2}$ . In the  $Y$  direction, the amplitude decreases from 1.71 to 0.79  $\text{m}\cdot\text{s}^{-2}$ . The frequency components are mainly the first and the second

natural frequency of the system. With the increase of frequency, the vibration response of the DGB 6205 system decreases. In addition, the natural frequency of the DGB 6205 system under time-varying load is ahead of that under constant load, indicating that the introduction of the time-varying load will lead to the forward shift of the natural frequency phase.

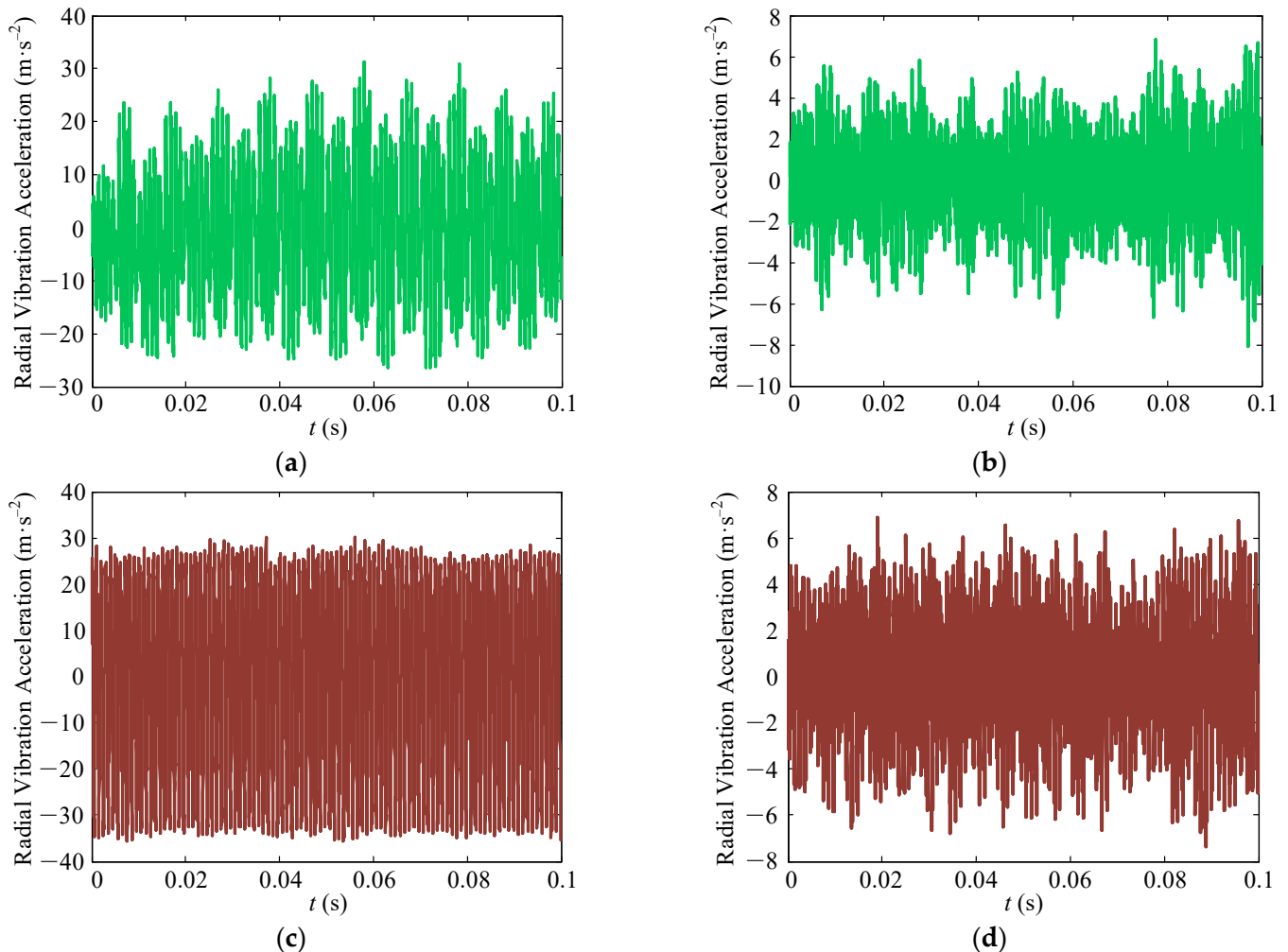


**Figure 10.** Vibration response of DGB 6205 system under time-varying load and constant load: (a) X-direction vibration response under time-varying load, (b) Y-direction vibration response under time-varying load, (c) X-direction vibration response under constant load, and (d) Y-direction vibration response under constant load.

#### 4.3. Sensitivity Analysis of DGB 6205 System Dynamic Response

The sensitivity of parameters to the dynamic response of the system is analyzed, and the influence law of different parameters on the dynamic characteristics of the system is revealed. To analyze the sensitivity of dynamic response of DGB 6205 system, the variation laws of radial displacement and radial vibration acceleration with speed  $n$  and radial clearance  $p$  are discussed respectively. The dynamic responses of DGB 6205 system under time-varying load and different parameters are obtained.

The variation law of radial displacement of DGB 6205 system with speed  $n$  and radial clearance  $p$  is shown in Figure 12.

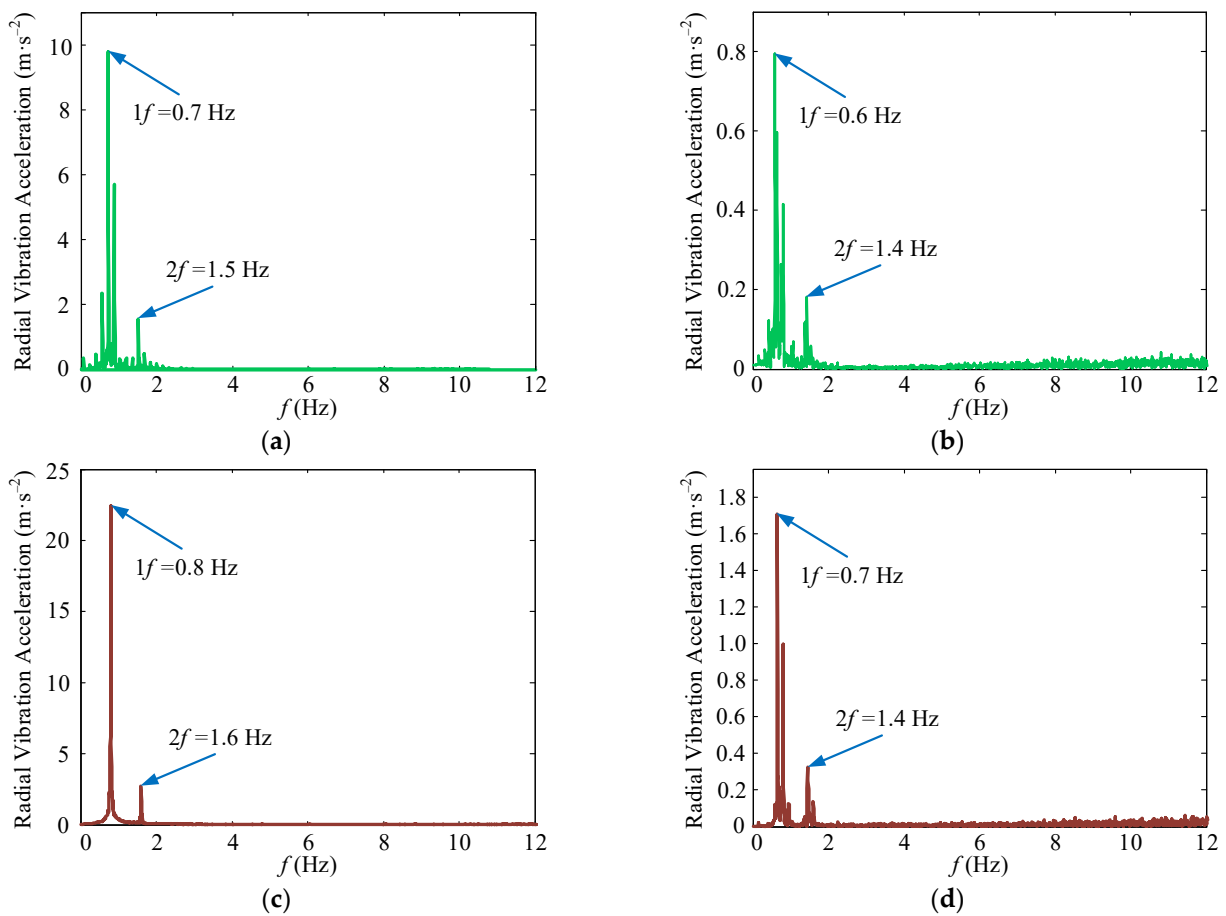


**Figure 11.** Vibration response of DGB 6205 system in the frequency domain: (a) X-direction frequency domain vibration response under time-varying load, (b) Y-direction frequency domain vibration response under time-varying load, (c) X-direction frequency domain vibration response under constant load, and (d) Y-direction frequency domain vibration response under constant load.

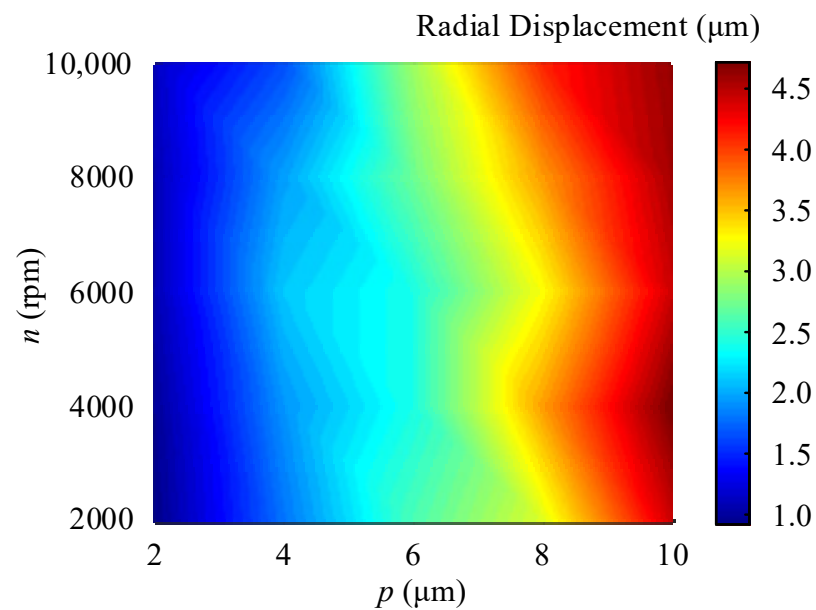


**Figure 12.** Variation law of radial displacement of DGB 6205 system with speed  $n$  and radial clearance  $p$ .

In Figure 12, it can be clearly seen that, as the radial clearance  $p$  increases from 2 to 10  $\mu\text{m}$ , the radial displacement response of DGB 6205 system gradually increases, indicating that the increase of radial clearance  $p$  will increase the radial displacement response of the system. Therefore, the dynamic response of the system is highly sensitive to the radial clearance  $p$ . However, as the speed  $n$  increases from 2000 to 10,000 rpm, the variation law of radial displacement response of the DGB 6205 system is not obvious, indicating that the sensitivity of the system's dynamic response to the speed  $n$  is low. In a certain range, the dynamic response of the system fluctuates slightly with the change of speed, because the change of speed causes the change of the natural frequency of the system.

The variation law of the radial vibration acceleration of the DGB 6205 system with speed  $n$  and radial clearance  $p$  is shown in Figure 13.

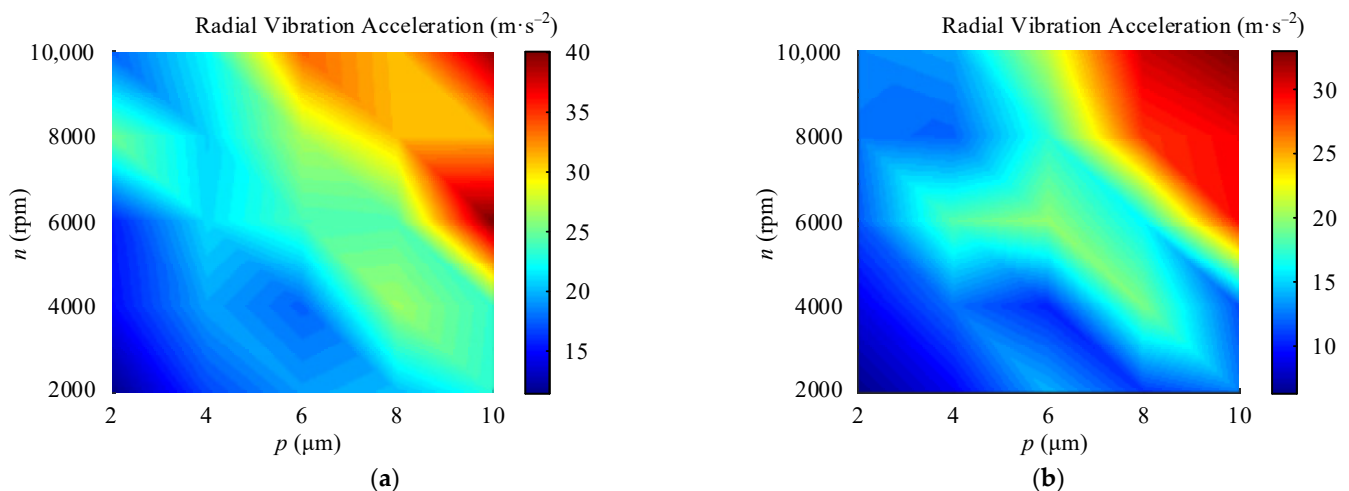


**Figure 13.** Variation law of radial vibration acceleration of the DGB 6205 system with speed  $n$  and radial clearance  $p$ : (a) X-direction radial vibration acceleration and (b) Y-direction radial vibration acceleration.

In Figure 13, as the radial clearance  $p$  increases from 2 to 10  $\mu\text{m}$ , the radial vibration acceleration response of the DGB 6205 system gradually increases. As the speed  $n$  increases from 2000 to 10,000 rpm, the radial vibration acceleration response of the DGB 6205 system increases gradually. It shows that the radial vibration acceleration response of the system is highly sensitive to the radial clearance  $p$  and speed  $n$ . The DGB 6205 system is more prone to slip at high speed, and the friction caused by the bearing slip increases the vibration response. With the change of radial clearance  $p$  and speed  $n$ , the amplitude of dynamic response of DGB 6205 system in the load action direction and perpendicular to the load action direction is different, but the change law of the system's dynamic characteristics is the same.

## 5. Conclusions

In this paper, the dynamic model of the DGB 6205 system, while considering the influence of sliding, was established, and the vibration characteristics of DGB 6205 system were analyzed. The slip characteristics of the DGB 6205 system, the influence of time-varying load on system dynamic response, and the sensitivity of system response to parameters were discussed, respectively. The conclusions can be drawn as follows:

- (1) The sliding speed between the ball and the inner raceway is greater than that between the ball and the outer raceway. With the increase of load  $F$ , the sliding speed of the ball and inner and outer raceways decreases gradually. The increase of speed  $n$  will lead to the increase of sliding speed, and the DGB 6205 system is more prone to the sliding phenomenon when operating at high speed.
- (2) Compared with the constant load condition, the radial vibration response of the DGB 6205 system under time-varying load is smaller. In the X direction, the root mean square value of radial vibration acceleration decreases from 20.17 to 11.81  $\text{m}\cdot\text{s}^{-2}$ . In

the Y direction, the root mean square value of radial vibration acceleration decreases from 2.20 to 1.81  $\text{m}\cdot\text{s}^{-2}$ .

- (3) With the increase of frequency, the amplitude of the dynamic response of the DGB 6205 system under constant load and time-varying load gradually decreases. At the same time, the introduction of the time-varying load will lead to the forward shift of the natural frequency phase.
- (4) The increase of radial clearance  $p$  will increase the dynamic response of the system. The dynamic response of the system is highly sensitive to the radial clearance  $p$ , and the sensitivity of the dynamic response of the system to the velocity  $n$  is lower than that of radial clearance  $p$ .

**Author Contributions:** F.L., software, conceptualization, data curation, and writing—original draft; X.L., formal analysis and writing—review and editing; D.S., validation and software. All authors have read and agreed to the published version of the manuscript.

**Funding:** This project was supported by the Fundamental Research Funds for the Central Universities (N2103025), the National Key Research and Development Program of China (2020YFB2007802), and the National Natural Science Foundation of China (Grant No. 51875092).

**Institutional Review Board Statement:** Not applicable.

**Informed Consent Statement:** Not applicable.

**Data Availability Statement:** Some data, models, or codes generated or used during the study are available from the corresponding author upon request.

**Conflicts of Interest:** The authors declare no conflict of interest.

## References

1. Harris, T.A. An analytical method to predict skidding in high speed roller bearings. *ASLE Trans.* **1966**, *9*, 229–241. [[CrossRef](#)]
2. Harris, T.A. An analytical method to predict skidding in thrust-loaded, angular-contact ball bearings. *J. Lubr. Technol.* **1971**, *93*, 17–23. [[CrossRef](#)]
3. Gupta, P.K. Dynamics of rolling-element bearings-part I: Cylindrical roller bearing analysis. *J. Lubr. Technol.* **1979**, *101*, 293–302. [[CrossRef](#)]
4. Gupta, P.K. Dynamics of rolling-element bearings-part II: Cylindrical roller bearing results. *J. Lubr. Technol.* **1979**, *101*, 305–311. [[CrossRef](#)]
5. Chen, W.; Ma, Z.; Liang, G.; Li, X.; Pan, J. Quasi-static analysis of thrust-loaded angular contact ball bearings. part I: Theoretical formulation. *Chin. J. Mech. Eng.* **2012**, *25*, 71–80. [[CrossRef](#)]
6. Chen, W.; Ma, Z.; Liang, G.; Li, X.; Pan, J. Quasi-static analysis of thrust-loaded angular contact ball bearings. part II: Results and discussion. *Chin. J. Mech. Eng.* **2012**, *25*, 81–87. [[CrossRef](#)]
7. Liao, N.T.; Lin, J.F. Ball bearing skidding under radial and axial loads. *Mech. Mach. Theory* **2002**, *37*, 91–113. [[CrossRef](#)]
8. Tu, W.; Shao, Y.; Mechefske, C.K. An analytical model to investigate skidding in rolling element bearings during acceleration. *J. Mech. Sci. Technol.* **2012**, *26*, 2451–2458. [[CrossRef](#)]
9. Shi, Z.; Liu, J. An improved planar dynamic model for vibration analysis of a cylindrical roller bearing. *Mech. Mach. Theory* **2020**, *153*, 103994. [[CrossRef](#)]
10. Han, Q.; Chu, F. Nonlinear dynamic model for skidding behavior of angular contact ball bearings. *J. Sound Vib.* **2015**, *354*, 219–235. [[CrossRef](#)]
11. Lin, C.J.; Jhang, J.Y. Bearing fault diagnosis using a grad-cam-based convolutional neuro-fuzzy network. *Mathematics* **2021**, *9*, 1502. [[CrossRef](#)]
12. Pan, Z.; Meng, Z.; Chen, Z.; Gao, W.; Shi, Y. A two-stage method based on extreme learning machine for predicting the remaining useful life of rolling-element bearings. *Mech. Syst. Signal Process.* **2020**, *144*, 106899. [[CrossRef](#)]
13. Huang, F.; Sava, A.; Adjallah, K.H.; Wang, Z. Fuzzy model identification based on mixture distribution analysis for bearings remaining useful life estimation using small training data set. *Mech. Syst. Signal Process.* **2021**, *148*, 107173. [[CrossRef](#)]
14. Kundu, P.; Darpe, A.K.; Kulkarni, M.S. Weibull accelerated failure time regression model for remaining useful life prediction of bearing working under multiple operating conditions. *Mech. Syst. Signal Process.* **2019**, *134*, 106302. [[CrossRef](#)]
15. Zhu, J.; Chen, N.; Shen, C. A new data-driven transferable remaining useful life prediction approach for bearing under different working conditions. *Mech. Syst. Signal Process.* **2020**, *139*, 106602. [[CrossRef](#)]
16. Li, F.; Li, X.; Guo, Y.; Shang, D. Analysis of contact mechanical characteristics of flexible parts in harmonic gear reducer. *Shock Vib.* **2021**, *2*, 5521320. [[CrossRef](#)]

17. Liu, J.; Shao, Y. Dynamic modeling for rigid rotor bearing systems with a localized defect considering additional deformations at the sharp edges. *J. Sound Vib.* **2017**, *398*, 84–102. [[CrossRef](#)]
18. Liu, J.; Shao, Y. A new dynamic model for vibration analysis of a ball bearing due to a localized surface defect considering edge topographies. *Nonlinear Dyn.* **2015**, *79*, 1329–1351. [[CrossRef](#)]
19. Niu, L.; Cao, H.; He, Z.; Li, Y. A systematic study of ball passing frequencies based on dynamic modeling of rolling ball bearings with localized surface defects. *J. Sound Vib.* **2015**, *357*, 207–232. [[CrossRef](#)]
20. Yang, Y.; Liu, C.; Jiang, D.; Behdinan, K. Nonlinear vibration signatures for localized fault of rolling element bearing in rotor-bearing-casing system. *Int. J. Mech. Sci.* **2020**, *173*, 105449. [[CrossRef](#)]
21. Yu, H.; Ran, Y.; Zhang, G.; Li, X.; Li, B. A time-varying comprehensive dynamic model for the rotor system with multiple bearing faults. *J. Sound Vib.* **2020**, *488*, 115650. [[CrossRef](#)]
22. Cao, H.; Su, S.; Jing, X.; Li, D. Vibration mechanism analysis for cylindrical roller bearings with single/multi defects and compound faults. *Mech. Syst. Signal Process.* **2020**, *144*, 106903. [[CrossRef](#)]
23. Ghafari, S.H.; Golnaraghi, F.; Ismail, F. Effect of localized faults on chaotic vibration of rolling element bearings. *Nonlinear Dyn.* **2008**, *53*, 287–301. [[CrossRef](#)]
24. Qin, Y.; Li, C.; Wu, X.; Wang, Y.; Chen, H. Multiple-degree-of-freedom dynamic model of rolling bearing with a localized surface defect. *Mech. Mach. Theory* **2020**, *154*, 104047. [[CrossRef](#)]
25. Gupta, P.K. Dynamic loads and cage wear in high-speed rolling bearings. *Wear* **1991**, *147*, 119–134. [[CrossRef](#)]